CONF-790889--2

RECENT WORK WITH FAST MOLECULAR-IONS AT ARGONNE NATIONAL LABORATORY

by

P.J. COONEY, D.S. GEMMELL, K.-O GROENEVELD, E.P. KANTER,
W.J. PIETSCH, Z. VAGER AND B.J. ZABRANSKY

Prepared for

Workshop on

PHYSICS WITH MOLECULAR-ION BEAMS

Argonne National Laboratory

Argonne, Illinois

August 20-21, 1979

U of C-AUA-USDOE

ARGONNE NATIONAL LABORATORY, ARGONNE, ILLINOIS

Operated under Contract W-31-109-Eng-38 for the
U. S. DEPARTMENT OF ENERGY

The facilities of Argonne National Laboratory are owned by the United States Government. Under the terms of a contract (W-31-109-Eng-38) among the U. S. Department of Energy, Argonne Universities Association and The University of Chicago, the University employs the staff and operates the Laboratory in accordance with policies and programs formulated, approved and reviewed by the Association.

MEMBERS OF ARGONNE UNIVERSITIES ASSOCIATION

The University of Arizona
Carnegie-Mellon University
Case Western Reserve University
The University of Chicago
University of Cincinnati
Illinois Institute of Technology
University of Illinois
Indiana University
The University of Iowa
Iowa State University
The University of Kansas
Kansas State University
Loyola University of Chicago
Marquette University
The University of Michigan
Michigan State University
University of Minnesota
University of Missouri
Northwestern University
University of Notre Dame
The Ohio State University
Ohio University
The Pennsylvania State University
Purdue University
Saint Louis University
Southern Illinois University
The University of Texas at Austin
Washington University
Wayne State University
The University of Wisconsin-Madison

Contribution to the workshop on Physics with Molecular-Ion Beams held at Argonne National Laboratory, 20-21 August 1979.

Recent Work with Fast Molecular-ion Beams at Argonne National Laboratory*

P. J. Cooney,** D. S. Gemmell, K.-O. Groeneveld,*** E. P. Kanter, W. J. Pietsch,† Z. Vager‡ and B. J. Zabransky

Physics Division, Argonne National Laboratory, Argonne, Illinois 60439

During the past year, we have invested our efforts primarily into the following areas:

a) Studies of molecular-ion dissociation in gaseous targets.

b) Developing an understanding of the origins of "central peaks" and of the two (as we believe, related) phenomena of the "transmission" of fast molecular ions through thin foil targets and of the production of neutral fragments from collision-induced dissociation of fast molecular projectiles.

c) Studies exploring the extent to which high-resolution measurements on dissociation fragments can be used to determine the steroechemical structures of the molecular ions in the incident beam.

d) Extensive modifications to the beam-line and apparatus at the 4-MV Dynamitron so as to permit a wide variety of coincidence measurements on fragments from collision-induced molecular-ion dissociation.

The apparatus that is currently in use at Argonne for these measurements is shown schematically in Fig. 1. Magnetically-analyzed molecular-ion beams from Argonne's 4-MV Dynamitron accelerator are collimated to have a maximum angular divergence of ±0.09 mrad at the target position. A set of "pre-deflector" plates permits electrostatic deflection of the beam incident on the target. Similarly, a set of "post-deflectors" is used to deflect charged particles emerging from the target. Charged particles entering the electrostatic analyzer are energy-analyzed with a relative resolution of $\pm 3 \times 10^{-4}$. The angular acceptance of the analyzer is ±0.11 mrad. Distributions in angle and energy are made for particles emerging from the target by varying the voltages on the pre-deflector and/or post deflector in conjunction with that on the analyzer. Neutrals are energy-analyzed by first stripping them in a ~100-Å thick carbon foil located just ahead of the analyzer. The overall angular resolution is ±0.15 mrad (0.008 degrees). Selection of the required charge state for particles leaving the target is facilitated by a suitable combination of pre- and post-deflection. The optimal combination also rejects spurious incident beams (e.g. pre-dissociated fragments arising from interactions in residual gas upstream from the target). Elaborate precautions are taken to ensure that no carbon buildup occurs on the target foils. A gas target can also be used in lieu of foils. For coincidence measurements, there are two movable (computer-controlled) detectors available in the detector chamber located upstream from the electrostatic analyzer (see Fig. 2).

Figures 3, 4 and 5 show typical distributions measured for H_2^+, HeH^+, and $^3He_2^+$ projectiles.

Figure 6 illustrates the manner in which parameters determined in the LAB frame are related to those in the COM frame. In the LAB frame, we measure the yield of a dissociation fragment as a function both of its angular shift (θ_x or equivalently, θ_y) from the direction of the incident beam (z-direction) and of its energy shift (ΔE) from the value $E = 1/2\ m_f V_o^2$ corresponding to the fragment's share of the projectile's kinetic energy (m_f is the fragment's mass, and $\vec{V}_o$ is the beam velocity). These LAB variables are related in a simple way to the asymptotic COM velocity $\vec{v}$ acquired by a fragment following the dissociation of a projectile. Since the momentum transfer is very small in most of the collisions leading to dissociation at these incident energies, we can assume that the projectile COM is undeflected in the collisions. If $\vec{V} = \vec{V}_o + \vec{v}$ is the asymptotic LAB velocity of the fragment, then, for $v \ll V_o$

$$\theta_x = v_x/V_o;\ \theta_y = v_y/V_o; \tag{1a}$$

$$\Delta E = 1/2\ m_f\ (V^2 - V_o^2) \approx m_f v_z V_o, \tag{1b}$$

and

$$\Delta E/E \approx 2v_z/V_o. \tag{1c}$$

The approximation in Eq. (1b) amounts to ignoring terms with relative magnitude $\sim v/V_o$ (typically, $v/V_o \sim 5 \times 10^{-3}$ for the cases considered here).

The (LAB) volume element in $(\theta_x, \theta_y, \Delta E/E)$ space is then

$$\tau = \delta\theta_x \delta\theta_y \delta(\Delta E/E) = 2V_o^{-3}\ \delta v_x \delta v_y \delta v_z. \tag{2}$$

That is, this LAB volume is directly proportional to the volume element in COM velocity space. This simple and convenient relationship is a consequence of the smallness of v/V_o; the vector $\vec{V}$ is almost parallel to $\vec{V}_o$ (Fig. 6) and so the transformation between LAB and COM frames, which in velocity space is a simple displacement of the origin by V_o, also amounts (to a good approximation) to a linear transformation between the LAB (θ_x, θ_y, $\Delta E/E$) frame and the COM velocity frame.

For a diatomic projectile, the Coulomb potential energy immediately after the loss of the binding electrons is $Z_1 Z_2 e^2/r$, where Z_1 and Z_2 are the effective charges on the ions as they begin to separate from an initial distance r. (For fast light ions and solid targets, Z_1 and Z_2 are very nearly equal to the atomic numbers of the fragments.) This Coulomb energy is typically several tens or even hundreds of eV. In comparison, we may normally neglect the small energies of vibrational and rotational motion that the projectile may possess at the beginning of the Coulomb explosion. The COM velocity subsequently achieved by a fragment of mass m_f is then

$$v = (1/m_f)\ (2\mu Z_1 Z_2 e^2/r)^{1/2} \tag{3}$$

where μ is the reduced mass. [In some cases, e.g. when treating dissociation in a gas target, it is obviously more appropriate to write Eq. (3) in terms of the proper dissociative potentials for the electronic states involved.]

From the foregoing, one sees that the diameter of an observed ring pattern is approximately proportional to the geometric mean of the effective charges on the fragments and inversely proportional to the square root of the

...nd length. Experiments with several species of diatomic molecular-ion projectiles[1-3] have established that the bond lengths obtained from such data agree well (typically within 0.01 Å) with calculated values when the effective charges Z_1 and Z_2 are chosen to have values that give the correct stopping power. The width of the "rim" of a ring pattern reflects the distribution $D(r)$ of the internuclear separations in the projectiles and this in turn is dependent upon the population of vibrational and electronic states in the incident beam.

Wake effects manifest themselves in slight distortions of the shape of a ring pattern and in a redistribution of the intensity around the ring. As is to be expected, the ring patterns observed for fragments arising from dissociation in gas targets show no sign of wake effects (e.g. Fig. 5). These patterns do however display a dominant central peak.

The first high-resolution measurements on foil-induced dissociation of energetic beams of HeH^+ revealed the presence of a small central peak in the ring pattern obtained for the resulting protons.[4] The authors suggested that this peak arises from the breakup mode $HeH^+ \rightarrow He^o + H^+$. Subsequently central peaks were reported[1] in the cases of H^+ from 3-MeV H_2^+ and 2.1-MeV H_3^+ and of $^3He^{++}$ from 3-MeV $^3He_2^+$ (all for thin foil targets). No central peaks were observed[1] for protons from 2.97-MeV OH_2^+ and 3.25-MeV CH^+ or for $^3He^+$ from 3-MeV $^3He_2^+$. Following this work, studies on the central peak observed for H^+ from the foil-induced dissociation of H_2^+ have been extended to both higher[5] and lower[3,6-8] beam energies. Figures 7 and 8 show some of the experimental data.

The central peak region in the cases of both gas and foil targets can be accounted for[3] in terms of those dissociations that produce one charged and one neutral fragment. For gas targets, this occurs via a collision-induced transition of the projectile to an excited electronic state which then decays dissociatively yielding a neutral and a charged fragment. Such processes are favored in the large-impact-parameter collisions that are possible in gases. For this type of excitation the resultant COM velocity acquired by the fragments can be small (~0.1 eV, say) if the initial internuclear separation is large [i.e. on the tail of the distribution $D(r)$]. Such fragments, although arising in only a small fraction of the dissociations, are detected for all initial projectile orientations and thus give rise to the large central peak.

For foil targets the central peak can originate in two main ways. For very thin foils corresponding to dwell times $\lesssim 10^{-16}$ sec a neutral fragment may originate and survive inside the foil. For thicker foils and longer dwell times a neutral and a charged fragment may be produced through capture of one or more electrons by one fragment at or near the point of exit from the foil. (Strictly speaking, the capture leads to the formation of a dissociative molecular state.) Inside the foil a normal Coulomb explosion develops. If the initial internuclear separation is large, the Coulomb explosion is weak and the fragments emerge with very low relative kinetic energy. This results in central peaks being observed in the ring patterns. The relative intensities of the central peaks are obviously sensitively dependent upon such factors as dwell time, $D(r)$, fragment charge, beam velocity, capture cross sections, etc. (for a fuller discussion, see Refs. 3, 6 and 9).

By performing coincidence measurements between H^+ and H^o from 290-keV H_2^+ bombarding a 2-ug/cm^2 carbon foil, Laubert and Chen[6] have elegantly demonstrated the connection between the H^+ central peak and the associated H^o.

A close inspection of the ring pattern for H^+ from foil-dissociated H_2^+ reveals[1] that the central peak is actually more like a central ridge than a peak (see also Fig. 3). The ridge extends in a direction corresponding to projectile orientations (referred to here as "transverse orientations") where the internuclear axis is approximately normal to the beam direction. We believe that this reflects an orientation-dependence of the electron-capture probability of the two protons as they emerge from the foil.

Further evidence for these orientation-dependent effects is to be found in the ring patterns measured for H^o atoms arising from the H_2^+ and HeH^+ bombardment of thin foils.[3] These patterns (Fig. 9) may be considered as consisting of two components: a) a central peak (a small central peak— not visible in Fig. 9— sits in the center of the pattern for HeH^+), and b) a ring that is enhanced for transverse orientations (or possibly reduced for in-line orientations). In the case of HeH^+, the orientation-dependence of the ring actually creates a dip in the forward direction. The rings correspond to Coulomb exploding diatomic clusters whose explosion is truncated at the exit surface by electron capture (the dependence of the ring diameter on target thickness confirms this). The central peaks for H^o are attributable to projectiles that lose their binding electrons, but do not explode appreciably in the target. These are incident projectiles having large initial internuclear separations. The neutral hydrogen then arises from capture at the exit surface. [For very short dwell times ($\gtrsim 10^{-16}$ sec) there may also be a contribution from neutrals whose electrons are contained in the incident projectile.]

If the electron capture at the exit surface takes place into a bound state of the emerging (but "non-exploding") ions a transmitted molecular ion may result. There is thus a direct correlation between the observation of central peaks and of transmission. Figure 10 shows the result of a measurement demonstrating that the internuclear separations for transmitted H_2^+ ions are indeed much larger than the average for the incident beam.

The relative smallness of the central peaks (Figs. 4 and 9) and of the transmission[1] for HeH^+ as compared with H_2^+, is a consequence of the narrowness of the potential well [and thus of the distribution D(r)] for HeH^+ as compared with H_2^+. In addition the higher nuclear charges and smaller equilibrium internuclear separation in HeH^+ produce a more rapid Coulomb explosion. A further factor is the necessity for capturing two electrons in the case of HeH^+ transmission or in the case of a central peak in the H^+ ring pattern for HeH^+ projectiles. Similar considerations explain the absence of both central peaks and transmission when thin foils are bombarded by CO^+, O_2^+, OH_2^+, OH^+, CH^+, etc.[1]

From an analysis of the ring patterns obtained with thin foil targets, one can determine D(r), the distribution of internuclear separations in the incident projectiles.[3] Figure 12 shows the population of vibrational states corresponding to the measured D(r) for an H_2^+ beam. It is evident that the incident beam is considerably "cooler" than would be expected, say, on the basis of a Franck-Condon distribution. This preferential population of the ground and low-lying vibrational states is characteristic of our measurements on a great variety of molecular-ion beams. Our measured D(r) are not detectably dependent on ion-source parameters over the range that these can be varied.

For dilute gas targets most collisions are much less violent than for foil targets. On the average fewer electrons are removed and there is thus a greater probability for dissociation into less highly charged fragments. One therefore expects to observe dissociation modes in which the molecular projectile, during a collision with a target atom or molecule, makes a vertical transition to an excited electronic state that then dissociates into separate fragments. (Vibrational excitation to continuum states is expected to be relatively infrequent at high projectile velocities.[11] Using the (known) potential curves shown in Fig. 12, and the distributions D(r) extracted from data obtained with foil targets, one can analyze the gas target data (e.g. Fig. 5) to determine the role played by various excited electronic states of the projectiles H_2^+ and HeH^+. We find that for H_2^+ about 90% of the dissociations proceed via the Coulomb (totally ionized) state and about 10% via the $2p\pi_u$ electronic state [leading to H^+ and H^o (n = 2)]. It would be interesting to perform beam-gas spectroscopy measurements with H_2^+ beams to verify that the n = 2 state in hydrogen is strongly populated. Analysis of the HeH^+ gas data is more complicated because a 2-electron projectile is inovlved. However the dissociation is clearly dominated by the He^+ (1s) + H^+ channel resulting from formation of the $1s\sigma$ electronic state of HeH^{++}.

High-resolution studies of fragments from the collision-induced dissociation of fast molecular-ion beams offer attractive possibilities for determining the stereochemistry of the projectiles. We have already noted[1] that bond lengths for several diatomic projectiles have been measured with

an accuracy of about 0.01 Å. Calculations indicate that for not-too-complicated molecular ions containing a small number of atoms, bond lengths and bond angles should be measurable to accuracies of about 0.01 Å and 1°, respectively. Although this level of accuracy is poor compared with that attainable with photon techniques (when they can be applied), it is sufficiently good to be of value in resolving many conflicts between predictions from structure calculations. Furthermore, this level of accuracy should be good enough to help practitioners of the photon techniques to zero in on the frequencies of their (usually very narrow) resonances. It is therefore of considerable interest to explore the extent to which these techniques with high-energy beams may be employed to determine the geometrical structures of polyatomic molecular-ion projectiles.

Following an initial joint experiment[12] with the University of Lyon and the Weizmann Institute on the structure of H_3^+, we at Argonne have made a series of studies on somewhat more complicated molecular-ion species. Figure 13 displays energy spectra for various charged fragments from 3.5-MeV CO_2^+ and N_2O^+ dissociating in carbon foils.[13] These molecular ions in their ground and low-lying states are known[14] to be linear; but while CO_2^+ has the symmetric form (O-C-O), N_2O^+ is asymmetric (N-N-O). From just a cursory inspection of the spectra in Fig. 13 (merely counting the peaks) one can immediately deduce the main features of these structures (i.e. their linearity and the order of atoms). Of course, to extract accurate bond lengths and angles, a much more detailed analysis is required. However, this example does point to the power of the technique in determining gross structures.

Figure 14 shows again how gross structure features are readily observed in such measurements— in this instance for the series CH_n^+ (n = 0— 4). Here one also sees clear evidence of the Jahn-Teller distortcn of the methane ion.

We have performed many measurements of this type— i.e. high-resolution studies of individual fragments in particular charge states. Except for very simple and/or highly symmetric ions (H_3^+, C_3^+, etc.) such measurements on single fragments yield only gross structure information. For example, our measurements on C^{2+} fragments from 3.6-MeV $C_3H_3^+$ ions dissociating in thin foils demonstrate only that the carbons sit on the corners of an approximately equilateral triangle. [That is, we have a beam of cyclopropenyl ions and not propargyl ions (which are linear in carbons).] Similarly, our measurements on single fragments from OH_2^+ show only that the protons are equivalent and that the oxygen is "in the middle". The accuracy in determining the bond length and bond angle is poor (~0.1 Å and ~10°, respectively).

For polyatomic ions, particularly those having low symmetry and/or many atomic constituents, the structures can be much more precisely determined if spatial and temporal coincidences can be recorded for two or more dissociation fragments from a given projectile. With this in mind, we recently revised the apparatus at Argonne so as to permit a wide variety of coincidence measurements (see Figs. 1 and 2). We can presently measure double or triple coincidences and record simultaneously information on fragment charge states, energies, and flight times from the target. The system has been tested with various simple diatomic and triatomic projectiles (H_2^+, HeH^+, CH^+, NH^+, OH^+, H_3^+, CH_2^+, NH_2^+, OH_2^+, etc.). Figure 15 shows a spatial scan of the proton-proton double coincidence rate for the foil-induced dissociation of 3.6-MeV OH_2^+ ions. Note that a given combination of

post-deflector and electrostatic analyzer voltage settings amounts to choosing for study a limited subset of the incoming projectile orientations. For the data shown in Fig. 15, only those OH_2^+ ions in which one proton is trailing ar selected. A simple analysis of these data gives the bond length to be 1.0 ± 0.04 Å and the H-O-H bond angle to be 110 ± 2° in agreement with results obtained from optical measurements[15] (the OH_2^+ ion is one of the eight polyatomic molecular ions whose structures have thus far been measured with photon techniques).

Although foil-induced dissociation has the virtue that essentially every incident projectile dissociates violently into individual highly charged monatomic ions, there are complications in the data analysis where one must take into account wake effects, target thickness, charge-state distributions, and multiple scattering. These problems do not arise if one uses a dilute gas target in which single collisions predominate. With gas targets however, there is the problem that most of the dissociations proceed through weak Coulomb explosions between ions having low charges. Also, the product fragments frequently include diatomic and polyatomic species. Thus the foil-induced and gas-induced dissociations tend to give complementary information and in studying any given projectile it is desirable to use both types of target. At Argonne we have recently begun triple coincidence measurements, e.g. on the pair of protons and the N^{3+} fragments arising from the dissociation of 3.6-MeV NH_2^+ ions in a dilute Ar gas jet. Although the triple coincidence counting rates are low, the data are very clean (Fig. 16 shows an example) and the analysis is greatly simplified as compared with the results obtained with foil targets.

References and Footnotes

*Work performed under the auspices of theDivision of Basic Energy Sciences of D.O.E.

**Visiting scientist 1978-78. Permanent address: Middlebury College, Middlebury, VT.

***Visiting scientist 1978. Permanent address: University of Frankfurt, W. Germany.

+Visiting scientist 1976-78. Permanent address: University of Cologne, W. Germany.

*Visiting scientist 1977, 1978 and 1979. Permanent address: Weizmann Institute of Science, Rehovoth, Israel.

[1] D. S. Gemmell, P. J. Cooney, W. J. Pietsch, A. J. Ratkowski, Z. Vager, B. J. Zabransky, A. Faibis, G. Goldring, and I. Levine, Proceedings of the 7th International Conference on Atomic Collisions in Solids, Moscow, Sept. 19—23, 1977, to be published.

[2] D. S. Gemmell, in Proceedings of the 6th International Congress on Radiation Research, Tokyo, Japan, May 13—18, 1979.

[3] E. P. Kanter, P. J. Cooney, D. S. Gemmell, K.-O. Groeneveld, W. J. Pietsch, A. J. Ratkowski Z. Vager, and B. J. Zabransky, Phys. Rev. A (to be published—September 1979).

[4] Z. Vager, D. S. Gemmell and B. J. Zabransky, Phys. Rev. A 14 (1976) 638.

[5] W. Pietsch, G. Krösing, G. Kumbartzki, and D. S. Gemmell (to be published).

[6] R. Laubert and F. K. Chen, Phys. Rev. Lett. 40, 174 (1978).

[7] M. J. Gaillard, J.-C. Poizat, and J. Remillieux, Phys. Rev. Lett. 41, 159 (1978).

[8] W. H. Escovitz, T. R. Fox and R. Levi-Setti, Proceedings of the 1978 Conference on the Applications of Small Accelerators in Research and Industry, IEEE Trans. Nucl. Sci., NS-26, 1147 (1979).

[9] Yu. Kagan, J. Phys. C (to be published).

[10] F. von Busch and G. H. Dunn, Phys. Rev. A 5, 1726 (1972).

[11] E. E. Salpeter, Proc. Phys. Soc. (London) 63A, 1295 (1950).

[12] M. J. Gaillard, D. S. Gemmell, G. Goldring, I. Levine, W. J. Pietsch, J.-C. Poizat, A. J. Ratkowski, J. Remillieux, Z. Vager, and B. J. Zabransky, Phys. Rev. A 17, 1797 (1978).

[13] D. S. Gemmell, E. P. Kanter, and W. J. Pietsch, Chem. Phys. Lett. 55, 331 (1978).

[14] G. Herzberg, Electronic spectra of polyatomic molecules (Van Nostrand, Princeton 1950).

[15] H. Lew and I. Heiber, J. Chem. Phys. 58, 1246 (1973).

Figure Captions

Fig. 1. Schematic diagram of the experimental arrangement at Argonne's 4-MV Dynamitron accelerator.

Fig. 2. Schematic diagram showing a cross-sectional view of the detector chamber and movable detector systems at Argonne's 4-MV Dynamitron accelerator.

Fig. 3. (a) Joint energy-angle distribution for protons arising from the dissociation of 1.4-MeV H_2^+ in an 88-Å thick carbon foil.[3]
(b) The corresponding energy spectrum of those protons emerging from the target foil in the beam direction.
(c) The corresponding angular distribution of the protons emerging from the target with an energy equal to that of the small central peak in (b).

Fig. 4. Joint energy-angle distributions for a) protons from 3.0-MeV HeH^+ dissociating in a 195-Å thick carbon foil and b) $^3He^{++}$ from 3.6-MeV $^3He_2^+$ dissociating in a 118-Å thick carbon foil.[2]

Fig. 5. Joint energy-angle distributions for protons from 1.2-MeV H_2^+ and 3.0-MeV HeH^+ dissociating in gaseous Ar (7.8 mTorr) and He (9.5 mTorr), respectively.[3]

Fig. 6. Kinematical relationships between the parameters (E,θ) measured for the outgoing molecular-ion fragment of mass m_f and its velocity $\vec{v}$ in the center-of-mass (COM) system moving along with the incident projectile.[3]

Fig. 7. Representative energy spectra of fragments from foil-induced Coulomb explosions.[1,4] (a) 3-MeV $H_2^+ \rightarrow H^+$; (b) 3.5-MeV $HeH^+ \rightarrow H^+$; (c) 3-MeV $^3He_2^+ \rightarrow {}^3He^{++}$; (d) 3-MeV $^3He_2^+ \rightarrow {}^3He^+$.

Fig. 8. Energy spectrum for protons emerging in the forward direction from a 4.2-μg/cm^2 carbon foil bombarded by a 27.55-MeV H_2^+ beam.[5] The dwell time of the ions in the target is 0.4 fsec.

Fig. 9. Ring patterns for (a) 3.0-MeV $H_2^+ \rightarrow H^o$ in a 132-Å carbon foil, and (b) 3.63-MeV $HeH^+ \rightarrow H^o$ in a 144-Å carbon foil.[3]

Fig. 10. Energy spectra of protons from 1-MeV $H_2^+ \rightarrow H^+$. The incident H_2^+ were first prepared by passage through a 330 Å carbon foil.

Fig. 11. Population distribution for the vibrational states of H_2^+ ions (shaded distribution) as deduced from the foil-induced dissociation of a 3.0-MeV H_2^+ beam. For comparison, the distributions expected from a Franck-Condon model and deduced from photo-dissociation experiments[10] are also shown.

Fig. 12 Interaction potentials used in fitting the c.m. velocity distributions of H^+ from (a) H_2^+ and (b) HeH^+ ion beams.[3]

Fig. 13. Zero-angle energy spectra for (a) O^{4+} and (b) C^{2+} resulting from 3.5-MeV CO_2^+ bombarding a 133 Å-thick C foil, and for (c) O^{4+} and (d) N^{3+} resulting from 3.5-MeV N_2O^+ bombarding a 160-Å thick C foil.[13]

Fig. 14. Energy widths measured for C^{4+} ions emerging at 0° from a 125-Å thick carbon foil bombarded by beams of CH_n^+ for n = 0–4. The beams all have the same velocity (corresponding to 194 keV/amu).

Fig. 15. Coincidence counting rate for protons from 3.6-MeV OH_2^+ dissociating in a 80-Å thick carbon foil. The rate is plotted as a function of the angle between the electrostatic analyzer (set on the low-energy, 0°, proton group) and one of the movable surface-barrier detectors (see Figs. 1 and 2).

Fig. 16. Top: H^+–N^{3+}–H^+ triple coincidence counting rate for 3.6-MeV NH_2^+ ions dissociating in an Ar gas-jet target. N^{3+} ions are detected at 0° in the electrostatic analyzer (Fig. 1). Protons are detected in the two movable detectors (Fig. 2). The coincidence rate is plotted as a function of the angle between the (symmetrically placed) proton detectors and the beam direction. Bottom: Same, but double coincidences (N^{3+} – H^+) obtained with a 70-Å carbon foil target. In both figures the total (energy-summed) proton-singles rates in the movable detectors are shown as dashed curves. In the top figure, the numbers (0,1,2,3) on the dashed curve refer to the corresponding nitrogen-ion charge state.

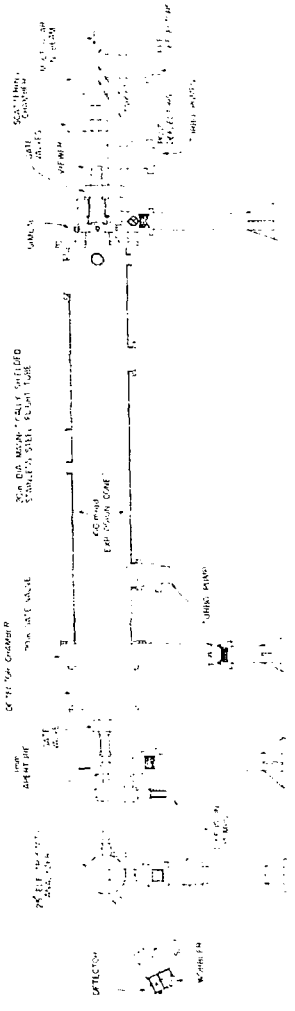

Fig. 1

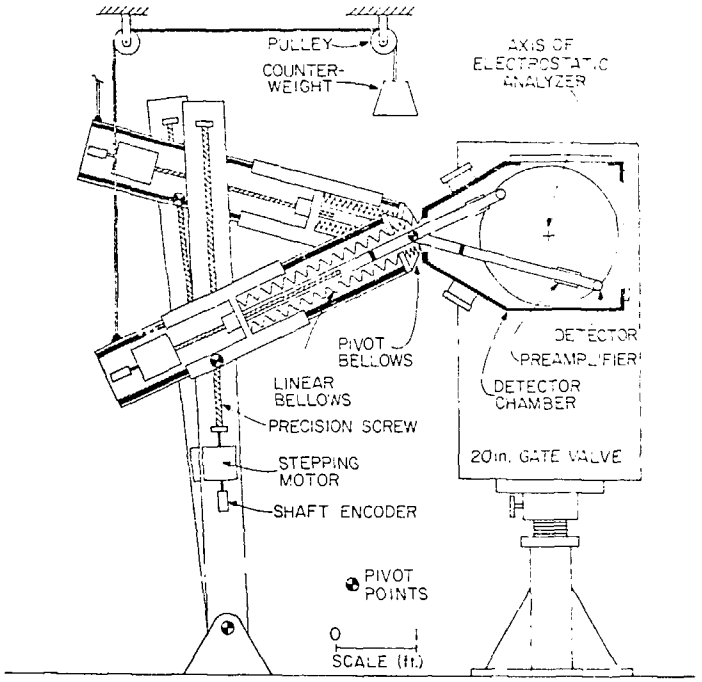
PULLEY
COUNTER-
WEIGHT
AXIS OF
ELECTROSTATIC
ANALYZER
PIVOT
BELLOWS
DETECTOR
PREAMPLIFIER
DETECTOR
CHAMBER
LINEAR
BELLOWS
PRECISION SCREW
20in. GATE VALVE
STEPPING
MOTOR
SHAFT ENCODER
PIVOT
POINTS
0
SCALE (ft.)

Fig. 2

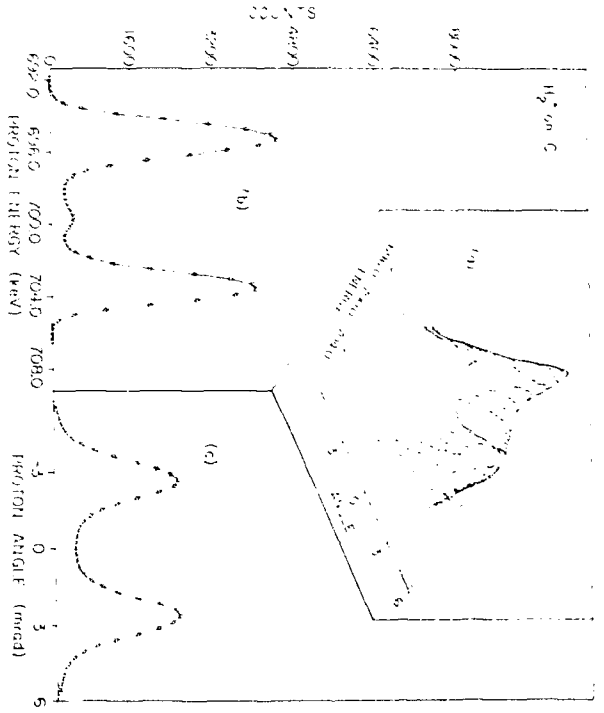

Fig. 3

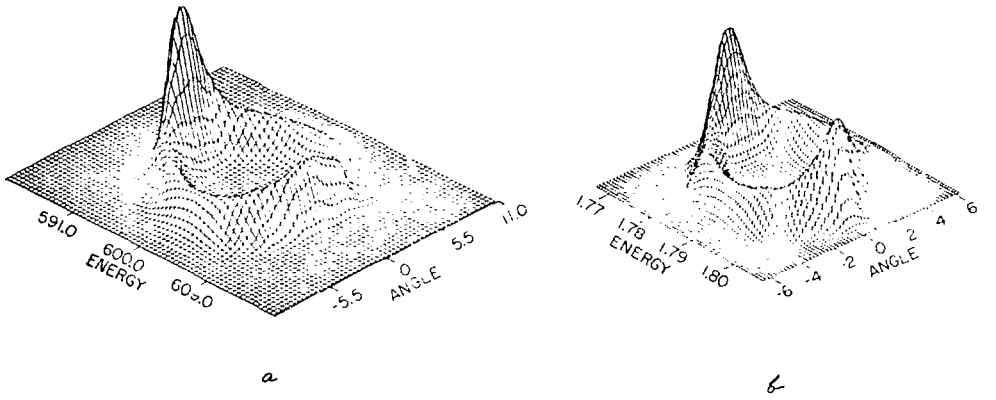
591.0
600.0
ENERGY
609.0
-5.5
0
ANGLE
5.5
11.0
a
1.77
1.78
ENERGY
1.79
1.80
-.6
-.4
-.2
0
.2
ANGLE
.4
.6
b

Fig. 4

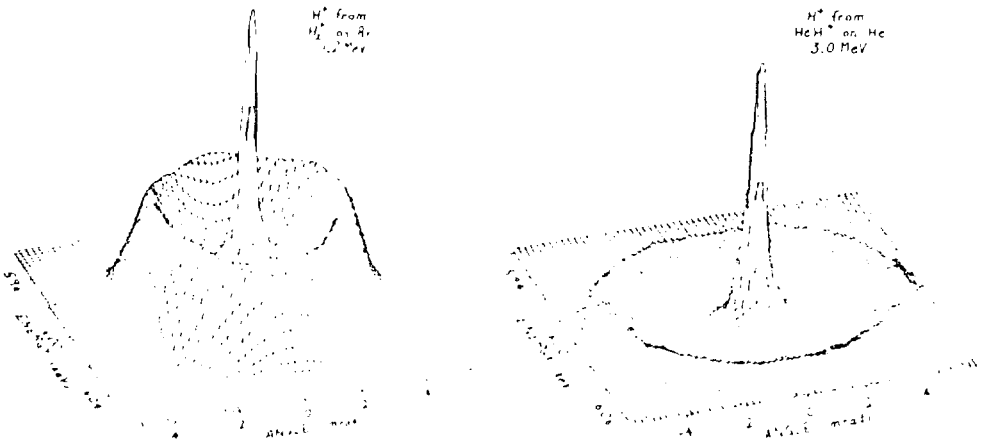
H+ from
H+ from
HeH+ on He
3.0 MeV

Fig. 5

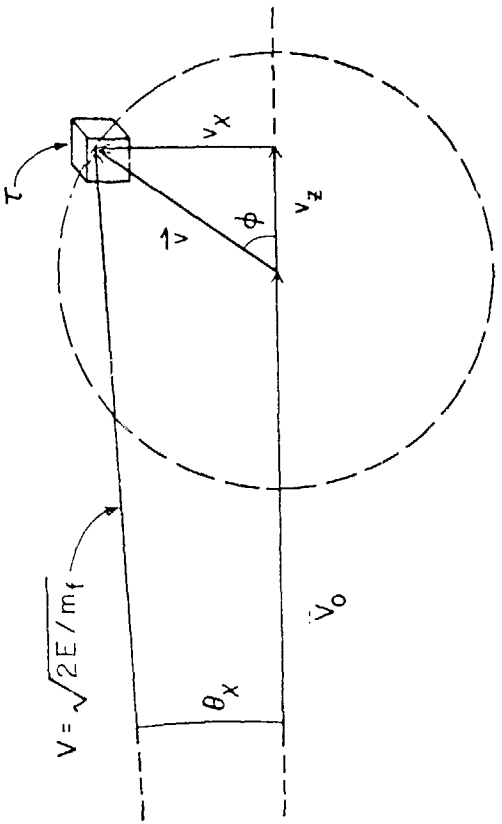
τ
v_x
v_z
$\vec{v}$
ϕ
V_o
$V = \sqrt{2E/m_f}$
θ_x

Fig. 6

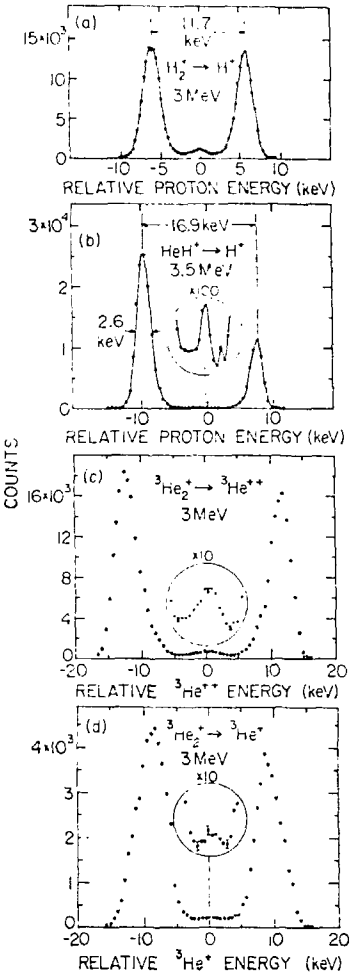
(a)
11.7 keV
$H_2^+ \rightarrow H^+$
3MeV
RELATIVE PROTON ENERGY (keV)
(b)
16.9keV
$HeH^+ \rightarrow H^+$
3.5MeV
x100
2.6 keV
RELATIVE PROTON ENERGY (keV)
COUNTS
(c)
$^3He_2^+ \rightarrow {}^3He^{++}$
3MeV
x10
RELATIVE $^3He^{++}$ ENERGY (keV)
(d)
$^3He_2^+ \rightarrow {}^3He^+$
3MeV
x10
RELATIVE $^3He^+$ ENERGY (keV)

Fig. 7

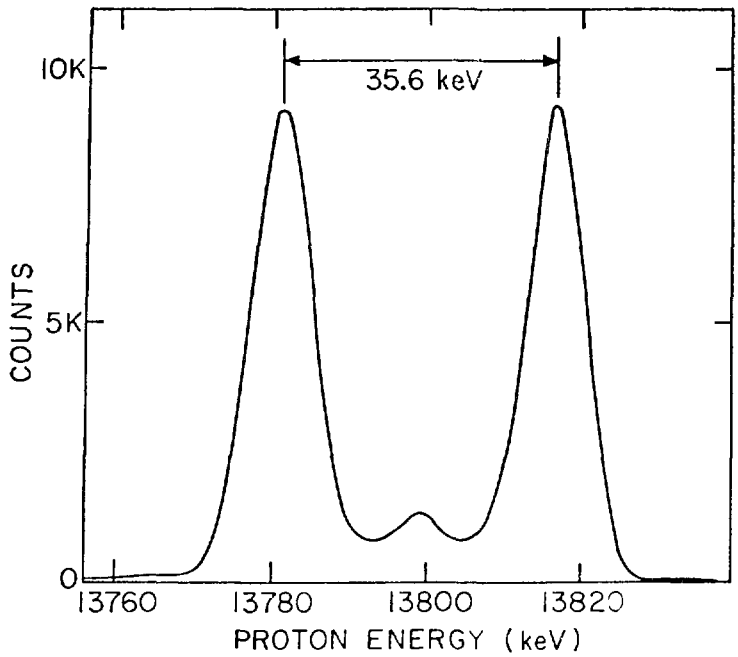
10K
5K
0
COUNTS
35.6 keV
13760
13780
13800
13820
PROTON ENERGY (keV)

Fig. 8

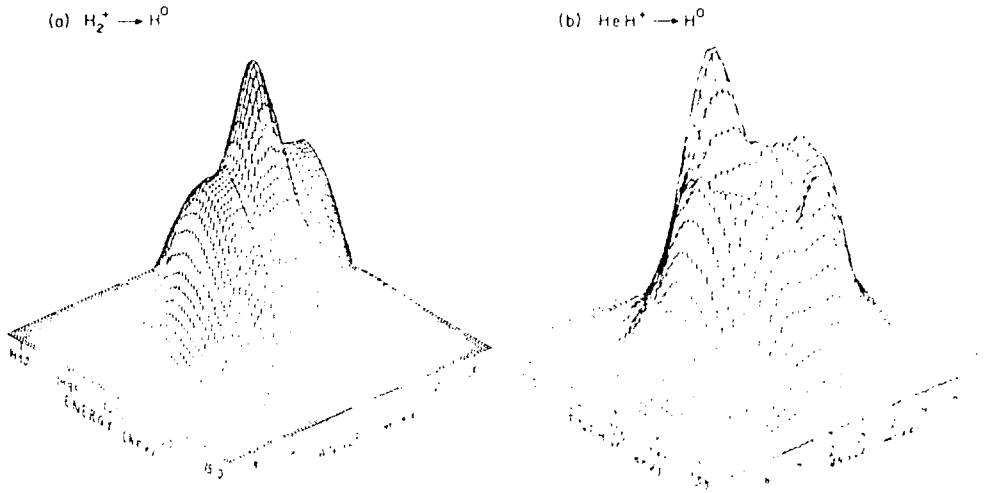
(a) $H_2^+ \longrightarrow H^0$
(b) $HeH^+ \longrightarrow H^0$

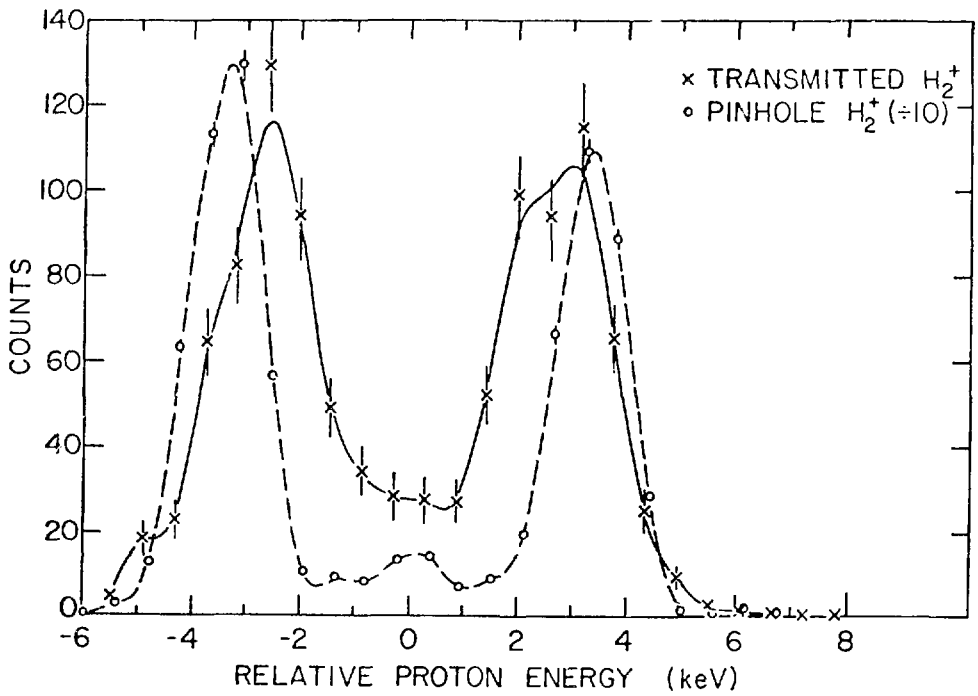
× TRANSMITTED H_2^+
∘ PINHOLE H_2^+ (÷10)
COUNTS
RELATIVE PROTON ENERGY (keV)

Fig. 10

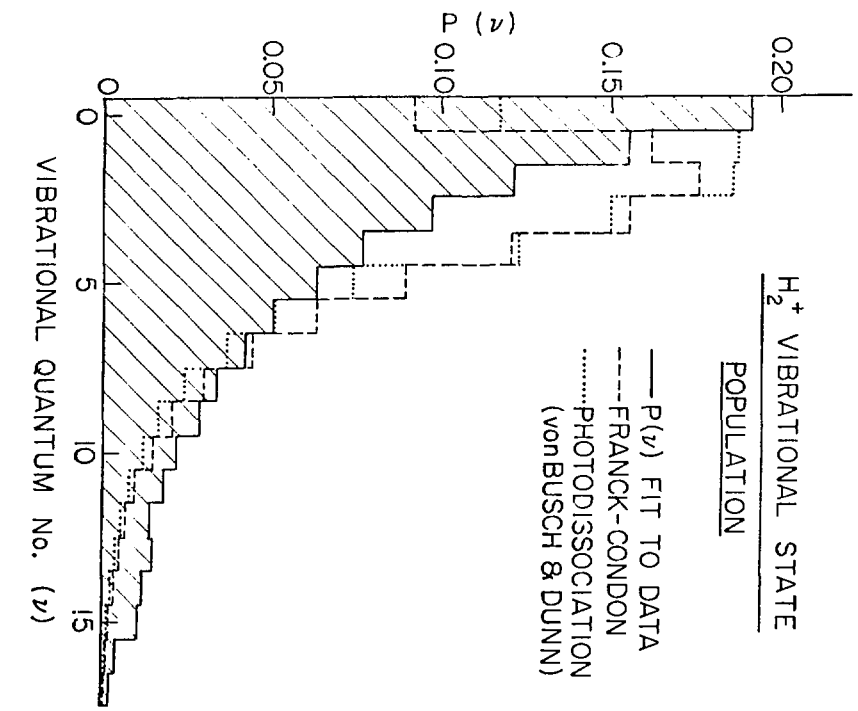
H_2^+ VIBRATIONAL STATE
POPULATION
—— P(ν) FIT TO DATA
---- FRANCK-CONDON
.....PHOTODISSOCIATION
(von BUSCH & DUNN)
P (ν)
VIBRATIONAL QUANTUM No. (ν)

Fig. 11

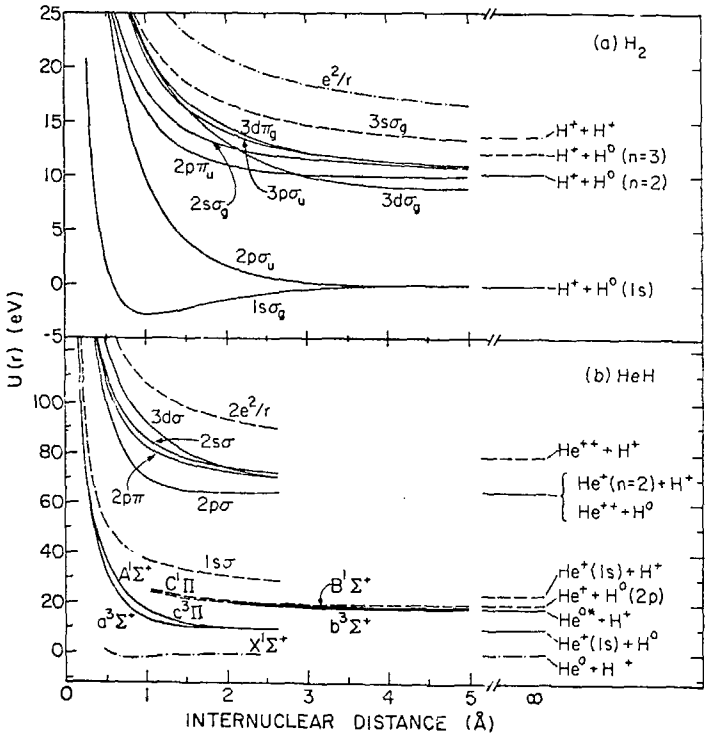
(a) H_2
e^2/r
$3s\sigma_g$
$3d\pi_g$
$2p\pi_u$
$2s\sigma_g$
$3p\sigma_u$
$3d\sigma_g$
$2p\sigma_u$
$1s\sigma_g$
$H^+ + H^+$
$H^+ + H^0$ (n=3)
$H^+ + H^0$ (n=2)
$H^+ + H^0$ (1s)
(b) HeH
$2e^2/r$
$3d\sigma$
$2s\sigma$
$2p\pi$
$2p\sigma$
$1s\sigma$
$A^1\Sigma^+$
$C^1\Pi$
$c^3\Pi$
$a^3\Sigma^+$
$X^1\Sigma^+$
$B^1\Sigma^+$
$b^3\Sigma^+$
$He^{++} + H^+$
$He^+(n=2) + H^+$
$He^{++} + H^0$
$He^+(1s) + H^+$
$He^+ + H^0(2p)$
$He^{a*} + H^+$
$He^+(1s) + H^0$
$He^0 + H^+$
U(r) (eV)
INTERNUCLEAR DISTANCE (Å)

Fig. 12

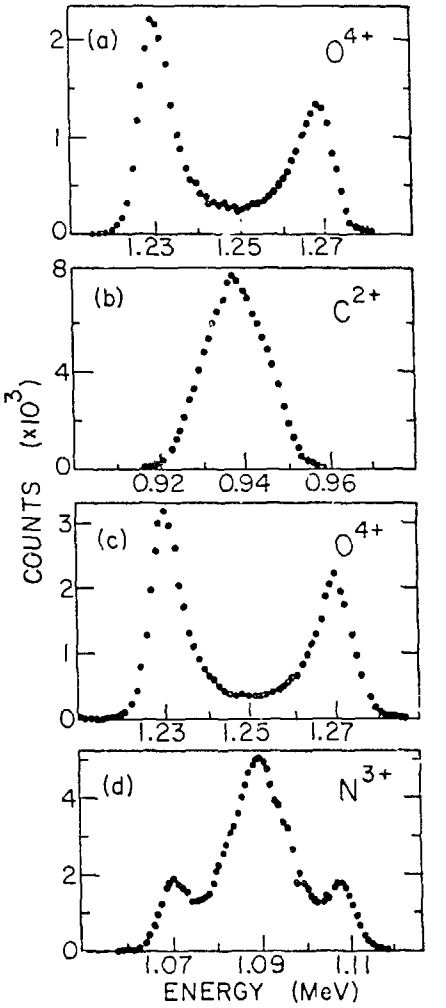
(a) O^{4+}
(b) C^{2+}
(c) O^{4+}
(d) N^{3+}
COUNTS (x10^3)
ENERGY (MeV)

Fig. 13

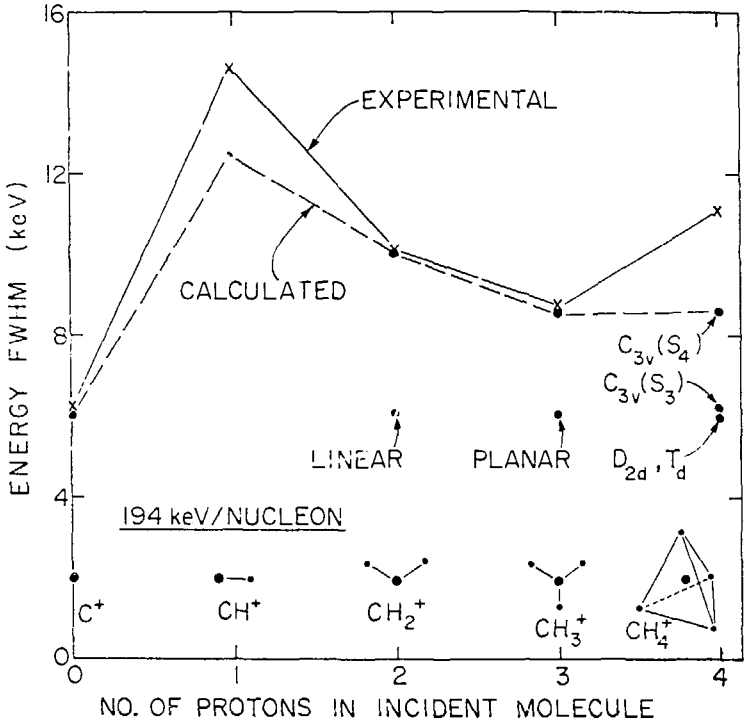
ENERGY FWHM (keV)
16
12
8
4
0
EXPERIMENTAL
CALCULATED
$C_{3v}(S_4)$
$C_{3v}(S_3)$
LINEAR
PLANAR
D_{2d}, T_d
194 keV/NUCLEON
C^+
CH^+
CH_2^+
CH_3^+
CH_4^+
0
1
2
3
4
NO. OF PROTONS IN INCIDENT MOLECULE

Fig. 14

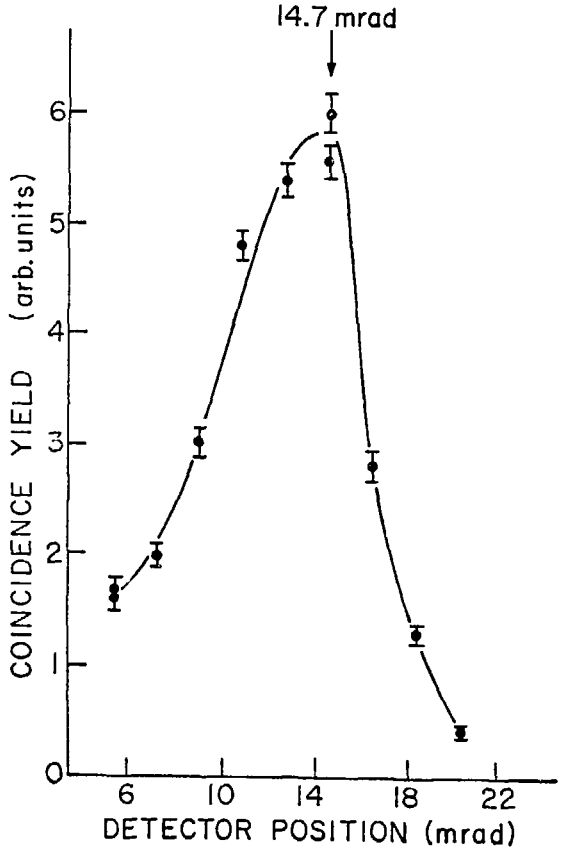
14.7 mrad
COINCIDENCE YIELD (arb. units)
6
5
4
3
2
1
0
6
10
14
18
22
DETECTOR POSITION (mrad)

Fig. 15

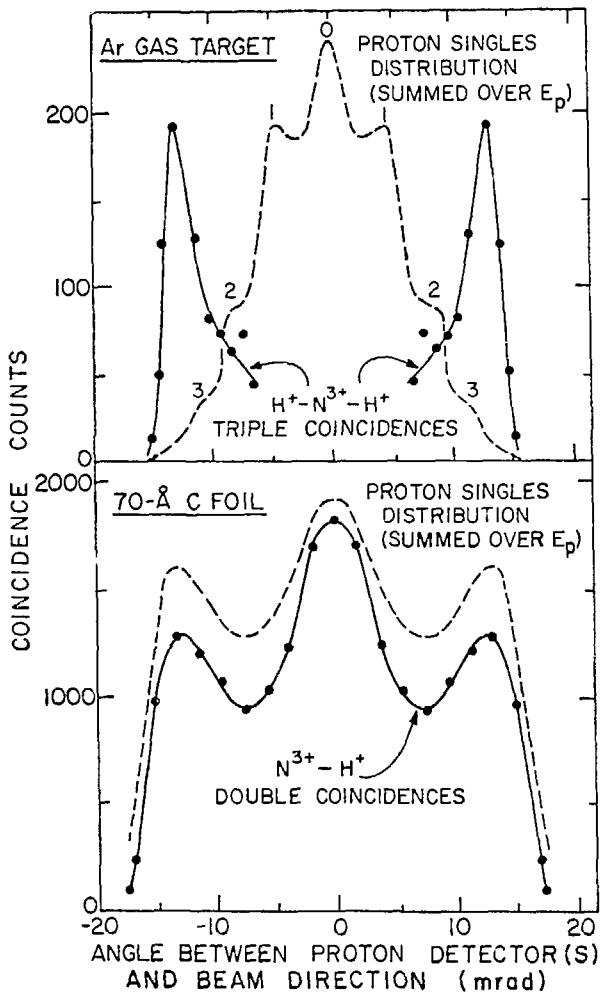
Ar GAS TARGET
PROTON SINGLES DISTRIBUTION (SUMMED OVER E_p)
0
2
2
3
3
$H^+ - N^{3+} - H^+$ TRIPLE COINCIDENCES
200
100
0
70-Å C FOIL
PROTON SINGLES DISTRIBUTION (SUMMED OVER E_p)
$N^{3+} - H^+$ DOUBLE COINCIDENCES
2000
1000
0
COINCIDENCE COUNTS
-20
-10
0
10
20
ANGLE BETWEEN PROTON DETECTOR(S) AND BEAM DIRECTION (mrad)

Fig. 16